Detection of single electron spin resonance in a double quantum dot*

F. H. L. Koppens,[a] C. Buizert, I. T. Vink, K. C. Nowack, T. Meunier, L. P. Kouwenhoven, and L. M. K. Vandersypen
Kavli Institute of NanoScience Delft, P.O. Box 5046, 2600 GA Delft, The Netherlands

Spin-dependent transport measurements through a double quantum dot are a valuable tool for detecting both the coherent evolution of the spin state of a single electron, as well as the hybridization of two-electron spin states. In this article, we discuss a model that describes the transport cycle in this regime, including the effects of an oscillating magnetic field (causing electron spin resonance) and the effective nuclear fields on the spin states in the two dots. We numerically calculate the current flow due to the induced spin flips via electron spin resonance, and we study the detector efficiency for a range of parameters. The experimental data are compared with the model and we find a reasonable agreement. © *2007 American Institute of Physics.*
[DOI: 10.1063/1.2722734]

I. INTRODUCTION

Recently, coherent spin rotations of a single electron were demonstrated in a double quantum dot device.[1] In this system, spin flips of an electron in the dot were induced via an oscillating magnetic field (electron spin resonance, or ESR) and detected through a spin-dependent transition of the electron to another dot, which already contained one additional electron. This detection scheme is an extension of the proposal for ESR detection in a single quantum dot by Engel and Loss.[2] Briefly, the device can be operated (in a spin blockade regime[3]) such that the electron in the left dot can only move to the right dot if a spin flip in one of the two dots is induced via ESR. From the right dot, the electron exits to the right reservoir and another electron enters the left dot from the left reservoir. A continuous repetition of this transition will result in a net current flow.

Compared to the single-dot detection scheme,[2] using the double dot as the detector has two major advantages. First, the experiment can be performed at a lower static magnetic field and consequently with lower, technically less demanding, excitation frequencies. Second, the spin detection is rather insensitive to unwanted oscillating electric fields, because the relevant dot levels can be positioned far from the Fermi energies of the leads. These electric fields are unavoidably generated together with the oscillating magnetic field as well.

The drawback of the double-dot detector is that spin detection is based on the projection in the two-electron singlet-triplet basis, while the aim is to detect single-spin rotations. However, this detection is still possible because the electrons in the two dots experience different effective nuclear fields.

This is due to the hyperfine interaction of the electron spins with the (roughly 10^6) nuclear spins in the host semiconductor material of each quantum dot.[4–11] In order to provide more insight into this double-dot ESR detection scheme for single-spin rotations, it is necessary to analyze the coherent evolution of the two-electron spin states together with the transitions in the transport cycle.

In this article, we discuss a model that describes the transport cycle in the spin blockade regime while including the coherent coupling between the two dots, and the influence of the static and oscillating magnetic field together with the effective nuclear fields on the electron spin states. The aim is to understand how effectively single-spin resonance will affect the measured quantity in the experiment, namely the current flow in the spin blockade regime. The organization of this article is as follows. First, we will explain the transport cycle and the mechanism that causes spin blockade. Next, we will briefly discuss the static system Hamiltonian and the mixing of the two-electron spin states by the effective nuclear field. Then, we add an oscillating magnetic field to this Hamiltonian, which forms—together with the double-dot tunneling processes—the basis of the rate equations that describe how the density matrix of the two-electron spin states evolves in time. The current flow, calculated from the steady state solution of the density operator, is then analyzed for different coherent coupling values, magnitudes of the oscillating magnetic field, in combination with different effective nuclear fields in the two dots. This provides further insight into the optimal conditions for spin flip detection with a double quantum dot.

II. SPIN BLOCKADE

In the spin-blockade regime, the double dot is tuned such that one electron always resides in the right dot, and a second electron can tunnel from the left reservoir through the left and right dots, to the right reservoir.[3] This current-carrying cycle can be described with the occupations (m,n) of the left and right dots: $(1,1) \rightarrow (0,2) \rightarrow (0,1) \rightarrow (1,1)$. When an electron enters the left dot and forms a double-dot singlet
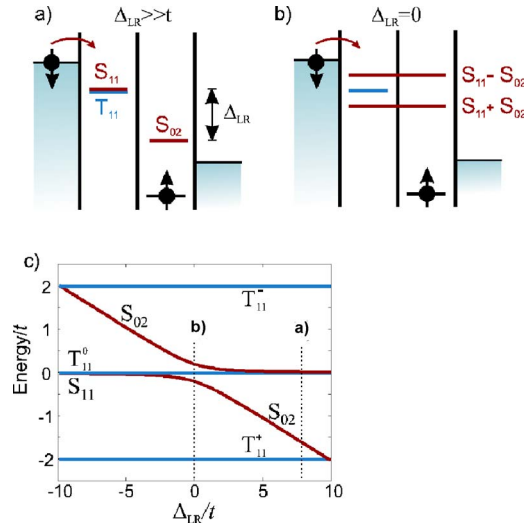

FIG. 1. (a) A schematic of the double dot and the electrochemical potentials [energy relative to the (0,1) state] of the relevant two-electron spin states. For $\Delta_{LR} > t$, transitions from the $|S_{11}\rangle$ state to the $|S_{02}\rangle$ state are possible via inelastic relaxation with rate Γ_{in}. Spin blockade occurs when one of the $|T_{11}^i\rangle$ states is occupied. (b) Similar schematic for $\Delta_{LR} = 0$, where the singlet states are hybridized. Also in this case, spin blockade occurs when one of $|T_{11}^i\rangle$ states is occupied. (c) Energy levels as a function of detuning. At $\Delta_{LR} = 0$, the singlet states hybridize into bonding and antibonding states. The splitting between the triplets states corresponds to the Zeeman energy $g\mu_B B_{ext}$.

state $|S_{11}\rangle$ with the electron in the right dot $|S\rangle = |\uparrow\downarrow\rangle - |\downarrow\uparrow\rangle$, normalization omitted for brevity), it is possible for the left electron to move to the right dot, because the right dot singlet state $|S_{02}\rangle$ is energetically accessible. Next, one electron tunnels from the right dot to the right lead and another electron can again tunnel into the left dot. If, however, the two electrons form a double-dot triplet state $|T_{11}^i\rangle$, the left electron cannot move to the right dot, as the right dot triplet state $|T_{02}\rangle$ is much higher in energy (due to the relatively large exchange splitting in a single dot). The electron also cannot move back to the lead; therefore further current flow is blocked as soon as any of the (double-dot) triplet states is formed [Figs. 1(a) and 1(b)].

Spin blockade only occurs if at least one of the eigenstates of the system Hamiltonian is a pure triplet state. If processes are present that induce transitions from all the three triplet states $|T_{11}^i\rangle$ to the singlet state $|S_{11}\rangle$ spin blockade is lifted and a current will flow. As we will see below, the presence of the nuclear spins in the host semiconductor can give rise to these kind of transitions. This can be seen most easily by adding the effect of the hyperfine interaction to the system Hamiltonian.

III. SYSTEM HAMILTONIAN

The system Hamiltonian is most conveniently written in the two-electron singlet-triplet basis with the quantization axis in the z-direction. The basis states are S_{11}, T_{11}^+, T_{11}^-, T_{11}^0, and S_{02}. The subscript m, n denotes the dot occupancy. We exclude the $|T_{02}\rangle$ state from the model, because this state is energetically inaccessible and therefore does not play an important role in the transport cycle. Furthermore, we neglect

the thermal energy kT in the description, which is justified when the bias over the two dots is much larger than kT. The system Hamiltonian is given by

$$H_0 = -\Delta_{LR}|S_{02}\rangle\langle S_{02}| + t(|S_{11}\rangle\langle S_{02}| + |S_{02}\rangle\langle S_{11}|)$$
$$- g\mu_B B_{ext}(|T_{11}^+\rangle\langle T_{11}^+| - |T_{11}^-\rangle\langle T_{11}^-|), \qquad (1)$$

where Δ_{LR} is the energy difference between the $|S_{11}\rangle$ and $|S_{02}\rangle$ state [level detuning, see Fig. 1(a)], t is the tunnel coupling between the $|S_{11}\rangle$ and $|S_{02}\rangle$ states, B_{ext} the external magnetic field in the z-direction. The eigenstates of the Hamiltonian Eq. (1) for finite external field are shown in Fig. 1(c). For $|\Delta_{LR}| < t$, the tunnel coupling t causes an anticrossing of the $|S_{11}\rangle$ and $|S_{02}\rangle$ states. For $\Delta_{LR} < 0$, transport is blocked by Coulomb blockade (i.e., the final state $|S_{02}\rangle$ is at a higher energy than the initial state $|S_{11}\rangle$). For $\Delta_{LR} \geq 0$, transport will be blocked when one of the three triplet states becomes occupied (spin blockade). In Figs. 1(a) and 1(b), we distinguish two regimes: $\Delta_{LR} \gg t$, where the (exchange) energy splitting between $|T_{11}^0\rangle$ and $|S_{11}\rangle$ is negligibly small and transitions from $|S_{11}\rangle$ to $|S_{02}\rangle$ occur via inelastic relaxation with rate Γ_{in}. A different regime holds for $|\Delta_{LR}| < t$, where $|S_{11}\rangle$ is coherently coupled with $|S_{02}\rangle$ giving rise to a finite (exchange) splitting between $|T_{11}^0\rangle$ and the hybridized singlet states. We will return to this distinction in the discussion below.

IV. SINGLET-TRIPLET MIXING BY THE NUCLEAR SPINS

The effect of the hyperfine interaction with the nuclear spins can be studied[12] by adding a static (frozen) effective nuclear field $\mathbf{B}_N^L$ ($\mathbf{B}_N^R$) at the left (right) dot to the system Hamiltonian,

$$H_{nucl} = -\frac{g\mu_B}{\hbar}(\mathbf{B}_N^L \cdot \mathbf{S}_L + \mathbf{B}_N^R \cdot \mathbf{S}_R)$$

$$= -\frac{g\mu_B}{\hbar}(\mathbf{B}_N^L - \mathbf{B}_N^R) \cdot (\mathbf{S}_L - \mathbf{S}_R)/2$$

$$- \frac{g\mu_B}{\hbar}(\mathbf{B}_N^L + \mathbf{B}_N^R) \cdot (\mathbf{S}_L + \mathbf{S}_R)/2, \qquad (2)$$

with $\mathbf{S}_{L(R)}$ the spin operator for the left (right) electron.

For the sake of convenience, we separate the inhomogeneous and homogeneous contributions, for reasons which we will discuss later. Considering the nuclear field as static is justified since the tunneling rates and electron spin dynamics are expected to be much faster than the dynamics of the nuclear system.[10,13,14] Therefore, we will treat the Hamiltonian as time independent. The effect of nuclear reorientation will be included later by ensemble averaging.

We will show now that triplet states mix with the $|S_{11}\rangle$ state if the nuclear field is different in the two dots (in all three directions). This mixing will lift spin blockade, detectable as a finite current running through the dots for $\Delta_{LR} \geq 0$. The effective nuclear field can be decomposed into a homogeneous and an inhomogeneous part [see the right-hand side of Eq. (2)]. The homogeneous part simply adds vectorially to the external field B_{ext}, changing slightly the Zeeman splitting
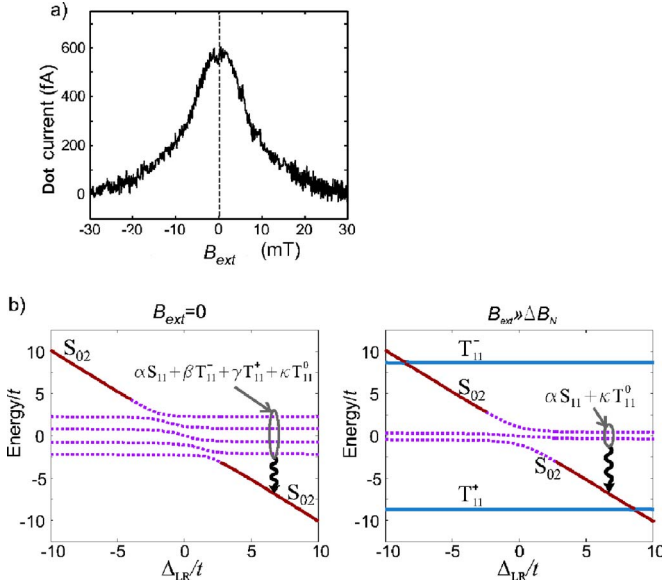
FIG. 2. (a) Observed current flow in the inelastic transport regime ($\Delta_{LR} \gg t$) due to singlet-triplet mixing by the nuclei. (b) Electrochemical potentials in the presence of H_{nucl} ($t \sim \Delta B_N$). Singlet and triplet eigenstates are denoted by red and blue lines, respectively. Hybridized states (of singlet and triplet) are denoted by dotted purple lines. For $g\mu_B B_{\text{ext}} \gg t$, $g\mu_B \Delta B_N$, the split-off triplets ($|T_{11}^+\rangle$ and $|T_{11}^-\rangle$) are hardly perturbed and current flow is blocked when they become occupied. Parameters: $t = 0.2$ μeV, $g\mu_B B_{N,L} = (0.1, 0, -0.1)$ μeV, $g\mu_B B_{N,R} = (-0.1, -0.2, -0.2)$ μeV, and $g\mu_B B_{\text{ext}} = 2$ μeV.

and preferred spin orientation of the triplet states. The inhomogeneous part $\Delta \mathbf{B}_N \equiv \mathbf{B}_N^L - \mathbf{B}_N^R$, on the other hand, couples the triplet states to the singlet state, as can be seen readily by combining the spin operators in the following way:

$$S_L^x - S_R^x = \frac{\hbar}{\sqrt{2}}(|S_{11}\rangle\langle T_{11}^-| - |S_{11}\rangle\langle T_{11}^+| + \text{H.c.}),$$

$$S_L^y - S_R^y = \frac{\hbar}{\sqrt{2}}(i|S_{11}\rangle\langle T_{11}^-| - i|S_{11}\rangle\langle T_{11}^+| + \text{H.c.}), \quad (3)$$

$$S_L^z - S_R^z = \hbar(|S_{11}\rangle\langle T_{11}^0| + |T_{11}^0\rangle\langle S_{11}|).$$

The first two expressions reveal that the inhomogeneous field in the transverse plane ΔB_N^x, ΔB_N^y mixes the $|T_{11}^+\rangle$ and $|T_{11}^-\rangle$ states with the $|S_{11}\rangle$. The longitudinal component ΔB_N^z mixes $|T_{11}^0\rangle$ with $|S_{11}\rangle$ (third expression). The degree of mixing between two states will depend strongly on the energy difference between them.[5] In the case of $g\mu_B B_{\text{ext}}$, $t < g\mu_B \sqrt{\langle \Delta B_N^2 \rangle}$, the three triplet states are close in energy to the $|S_{11}\rangle$ state. Their intermixing will be strong, lifting spin blockade. For $g\mu_B B_{\text{ext}} \gg t$, $g\mu_B \sqrt{\langle \Delta B_N^2 \rangle}$ the $|T_{11}^+\rangle$ and $|T_{11}^-\rangle$ states are split off in energy by an amount of $g\mu_B B_{\text{ext}}$. Consequently, the perturbation of these states caused by the nuclei will be small. Although the $|T_{11}^0\rangle$ remains mixed with the $|S_{11}\rangle$ state, the occupation of one of the two split-off triplet states can block the current flow through the system.

The effect of nuclear mixing is shown in Fig. 2.[5] The observed current flow through the system is typically on the order of a few hundreds of fA [Fig. 2(a)]. At zero field, where the mixing is strongest, the current flow is largest. Increasing the field gradually restores spin blockade. Figure

2(b) shows the energy levels for zero and finite external field. The theoretical calculations of the nuclear-spin mediated current flow (obtained from a master equation approach) are discussed in Refs. 12 and 15.

V. OSCILLATING MAGNETIC FIELD AND RATE EQUATIONS

So far, we have seen that the occurrence of transitions between singlet and triplet spin states is detectable as a small current in the spin-blockade regime. We will now discuss how this lifting of spin blockade can also be used to detect single-spin rotations, induced via electron spin resonance. The basic idea is the following. If the system is blocked in e.g., $|\uparrow\uparrow\rangle$, and the driving field rotates, e.g., the left spin, then transitions are induced to the state $|\downarrow\uparrow\rangle$. This state contains a singlet component and therefore a probability for the electron to move to the right dot and right lead. Inducing single-spin rotations can therefore lift spin blockade.

However, together with the driving field, the spin transitions are much more complicated due to the interplay of different processes: spin resonance of the two spins, interaction with the nuclear fields, spin state hybridization by coherent dot coupling, and inelastic transitions from the $|S_{11}\rangle$ state to the $|S_{02}\rangle$ state. In order to understand the interplay of these processes, we will first model the system with a time-dependent Hamiltonian and a density matrix approach. Next, we will discuss the physical interpretation of the simulation results.

The Hamiltonian now also contains a term with an oscillating magnetic field in the x-direction with amplitude B_{ac},

$$H_{\text{ac}}(t) = \frac{g\mu_B B_{\text{ac}}}{\hbar}\sin(\omega\tau)(S_L^x + S_R^x). \quad (4)$$

We assume that B_{ac} is equal in both dots, which is a reasonable approximation in the experiment (from simulations we find that the difference of B_{ac} is 20% at most[1]). We assume $B_{\text{ext}} \gg B_N$, B_{ac}, which allows application of the rotating wave approximation.[16] Therefore, we will define $B_1 \equiv \frac{1}{2}B_{\text{ac}}$, which is in the rotating frame the relevant driving field for the ESR process.

In order to study the effect of ESR and the nuclear fields that are involved in the transport cycle, we will construct rate equations that include the unitary evolution of the spins in the dots governed by the time-dependent Hamiltonian. This approach is based on the model of Ref. 12, where the Hamiltonian contained only time-independent terms. Seven states are involved in the transport cycle, namely the three triplets $|T_{11}^i\rangle$, the singlet states $|S_{11}\rangle$ and $|S_{02}\rangle$, and the two (0,1) states $|\uparrow_{01}\rangle$ and $|\downarrow_{01}\rangle$, making the density operator a 7×7 matrix. The rate equations based on the time-independent Hamiltonian are given in Ref. 12. These are constructed from the term that gives the unitary evolution of the system governed by the Hamiltonian ($H = H_0 + H_{\text{ac}}$) $d\hat{\rho}_k/d\tau = -(i/\hbar) \times \langle k|[H, \hat{\rho}]|k\rangle$, together with terms that account for incoherent tunneling processes between the states. The rate equations for the diagonal elements are given by

$$\frac{d\hat{\rho}_{T_{11}^+}}{d\tau} = -\frac{i}{\hbar}\langle T_{11}^+|[H,\hat{\rho}]|T_{11}^+\rangle + \frac{\Gamma_L}{2}\hat{\rho}_{\uparrow_{01}},$$

$$\frac{d\hat{\rho}_{T_{11}^-}}{d\tau} = -\frac{i}{\hbar}\langle T_{11}^-|[H,\hat{\rho}]|T_{11}^-\rangle + \frac{\Gamma_L}{2}\hat{\rho}_{\downarrow_{01}},$$

$$\frac{d\hat{\rho}_{T_{11}^0}}{d\tau} = -\frac{i}{\hbar}\langle T_{11}^0|[H,\hat{\rho}]|T_{11}^0\rangle + \frac{\Gamma_L}{4}(\hat{\rho}_{\uparrow_{01}} + \hat{\rho}_{\downarrow_{01}}),$$

$$\frac{d\hat{\rho}_{S_{11}}}{d\tau} = -\frac{i}{\hbar}\langle S_{11}|[H,\hat{\rho}]|S_{11}\rangle + \frac{\Gamma_L}{4}(\hat{\rho}_{\uparrow_{01}} + \hat{\rho}_{\downarrow_{01}}) - \Gamma_{in}\hat{\rho}_{S_{11}},$$

$$\tag{5}$$

$$\frac{d\hat{\rho}_{S_{02}}}{d\tau} = -\frac{i}{\hbar}\langle S_{02}|[H,\hat{\rho}]|S_{02}\rangle + \Gamma_{in}\hat{\rho}_{S_{11}} - \Gamma_R\hat{\rho}_{S_{02}},$$

$$\frac{d\hat{\rho}_{\uparrow_{01}}}{d\tau} = +\frac{\Gamma_R}{2}\hat{\rho}_{S_{02}} - \Gamma_L\hat{\rho}_{\uparrow_{01}},$$

$$\frac{d\hat{\rho}_{\downarrow_{01}}}{d\tau} = +\frac{\Gamma_R}{2}\hat{\rho}_{S_{02}} - \Gamma_L\hat{\rho}_{\downarrow_{01}}.$$

The rate equations for the off-diagonal elements are given by

$$\frac{d\hat{\rho}_{jk}}{d\tau} = -\frac{i}{\hbar}\langle j|[H,\hat{\rho}]|k\rangle - \frac{1}{2}(\Gamma^j + \Gamma^k)\hat{\rho}_{jk}, \tag{6}$$

where the indices $j,k \in \{T_{11}^i, S_{11}, S_{02}, \uparrow_{01}, \downarrow_{01}\}$ label the states available to the system. The tunneling/projection rates Γ^j equal Γ_{in} and Γ_R for the $|S_{11}\rangle$ and $|S_{02}\rangle$ states, respectively, and equal zero for the other five states. The first term on the right-hand side describes the unitary evolution of the system, while the second term describes a loss of coherence due to the finite lifetime of the singlet states. This is the first source of decoherence in our model. The second one is the inhomogeneous broadening due to the interaction with the nuclear system. We do not consider other sources of decoherence, as they are expected to occur on much larger time scales.

Because we added a time-dependent term to the Hamiltonian (the oscillating field), we numerically calculate the time evolution of $\hat{\rho}(t)$, treating the Hamiltonian as stationary on the time scale $\Delta\tau \ll 2\pi/\omega$. To reduce the simulation time, we use the steady-state solution $\hat{\rho}_{\tau \to \infty}$ in the absence of the oscillating magnetic field as the initial state $\hat{\rho}(\tau=0)$ for the time evolution. At $\tau=0$ the oscillating field is turned on and the system evolves toward a dynamic equilibrium on a time scale set by the inverse of the slowest tunneling rate Γ. This new equilibrium distribution of populations is used to calculate the current flow, which is proportional to the occupation of the $|S_{02}\rangle$ state ($I = e\Gamma_R\hat{\rho}_{S_{02}}$). An example of the time evolution of the density matrix elements is shown in Fig. 3. The figure clearly reveals that the blockade is lifted when the oscillating field is applied. This is visible as an increase of the occupation of the $|S_{02}\rangle$ state.
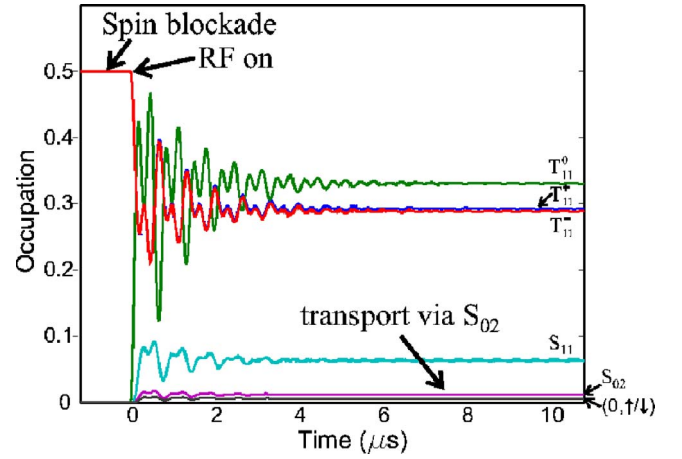

FIG. 3. Time evolution of the diagonal elements of the density matrix for one particular nuclear configuration. Parameters: $\hbar\omega = g\mu_B 100$ mT, $B_{ext} = 100$ mT, $B_{N,x,y,z}^L = (0,0,2.2)$ mT, $B_{N,x,y,z}^R = (0,0,0)$, $B_1 = 1.3$ mT, $\Gamma_L = 73$ MHz, $\Gamma_R = 73$ MHz, $\hbar\Gamma_{in} = g\mu_B B_{N,z}^L$ and $\Delta_{LR} = 200$ μeV, $t = 0.3$ μeV.

In order to simulate the measured current flow, we have to consider the fact that the measurements are taken with a sampling rate of 1 Hz. As the time scale of the nuclear dynamics is believed to be much faster than 1 Hz,[10,13,14] we expect each data point to be an integration of the response over many configurations of the nuclei. The effect of the evolving nuclear system is included in the calculations by averaging the different values of the (calculated) current flow obtained for each frozen configuration. These configurations are randomly sampled from a Gaussian distribution of nuclear fields in the left and right dot (similar as in Ref. 12). Because the electrons in the two dots interact with different nuclear spins, the isotropic Gaussian distributions in the two dots are uncorrelated, such that $\sqrt{\langle \Delta B_N^2 \rangle} = \sqrt{2}\sqrt{\langle B_N^2 \rangle}$ and $\langle B_{N,x}^2 \rangle = \langle B_{N,y}^2 \rangle = \langle B_{N,z}^2 \rangle$. For the sake of convenience, we define

$$\sigma_N = \sqrt{\langle B_N^2 \rangle} \quad \text{and} \quad \sigma_{N,z} = \sqrt{\langle B_{N,z}^2 \rangle} = \sqrt{\frac{1}{3}\langle B_N^2 \rangle}. \tag{7}$$

VI. SIMULATION RESULTS AND PHYSICAL PICTURE

An example of the calculated (average) current flow as a function of B_{ext} [Figs. 4(a) and 4(b)] shows a (split) peak around zero magnetic field and two satellite peaks for $B_{ext} = \pm\hbar\omega/(g\mu_B)$, where the spin resonance condition is satisfied. This (split) peak at $B_{ext}=0$ is due to singlet-triplet mixing by the inhomogeneous nuclear field, and the splitting depends on the tunnel coupling, similar as the observations in Ref. 5. The response from the induced spin flips via the driving field is visible for the both inelastic and resonant transport regime, and the current flow has comparable magnitude to the peak at $B_{ext}=0$. The satellite peaks are also visible in the experimental data from Ref. 1 (also shown here in Fig. 4), although the shape and width of the satellite peaks are different, as we will discuss later.

We want to stress that the ESR satellite peaks only appear when an inhomogeneous nuclear field is present in the simulations. In other words, for $\Delta B_N=0$ and B_1 equal in both dots, spin rotations are induced in both dots at the same time
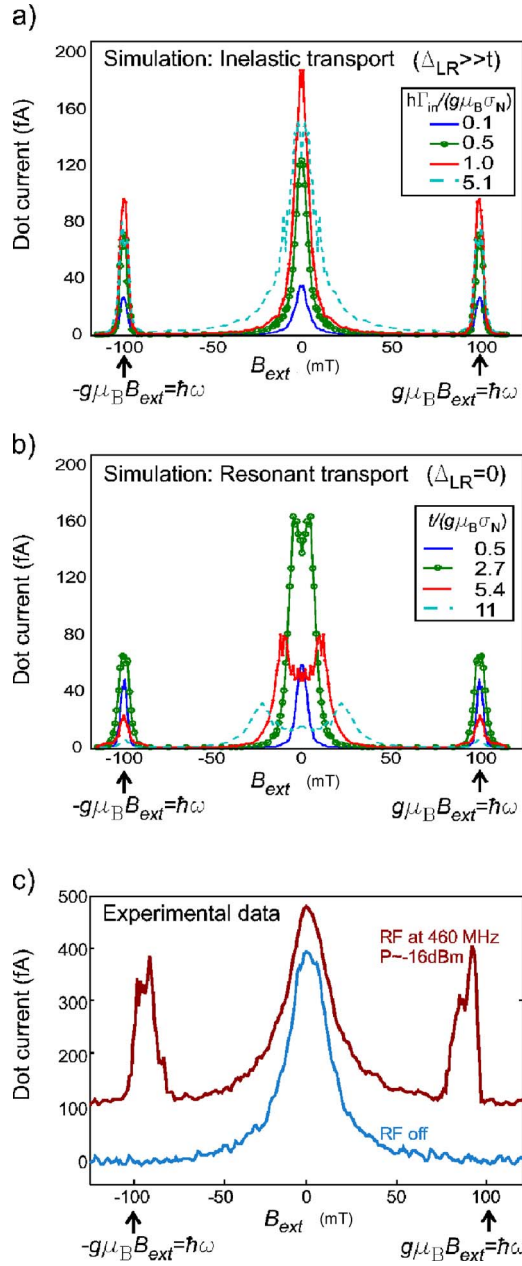
FIG. 4. (a). Calculated average current flow in the inelastic transport regime. Parameters: $\hbar\omega = g\mu_B 100$ mT, $B_{ext}=100$ mT, $\sigma_N=2.2$ mT, $B_1=1.3$ mT, $\Gamma_{L,R}=73$ MHz, $t=0.3$ μeV, and $\Delta_{LR}=200$ μeV. Results are similar for any value for t, provided that $\Delta_{LR}\gg t$. b) Calculated average current flow in the resonant transport regime at zero detuning for different values of t. Parameters: $\hbar\omega=g\mu_B 100$ mT, $\sigma_N=2.2$ mT, $B_1=1.3$ mT, $\Gamma_{L,R}=73$ MHz, $\Gamma_{in}=0$, and $\Delta_{LR}=0$, averaged over 400 nuclear configurations for $t/(g\mu_B\sigma_N)>0.5$ and 60 configurations for $t/(g\mu_B\sigma_N)=0.5$. Simulations carried out for positive magnetic fields only; values shown for negative fields are equal to results obtained for positive field. (c) Experimental data from Ref. 1 with (curve offset by 100 fA for clarity) and without oscillating magnetic field. The frequency of the oscillating magnetic field is 460 MHz and the applied power is −16 dBm.

and at the same rate. Starting, for example, from the state $|T_{11}^+\rangle=|\uparrow\uparrow\rangle$, transitions are induced to the state $|\downarrow\downarrow\rangle$ via the intermediate state $(|\uparrow\rangle+|\downarrow\rangle)(|\uparrow\rangle+|\downarrow\rangle)/\sqrt{2}=(|T_{11}^+\rangle+|T_{11}^-\rangle +2|T_{11}^0\rangle)/\sqrt{2}$. No mixing with the singlet state takes place (the evolution is in the triplet subspace), and no current will therefore flow.
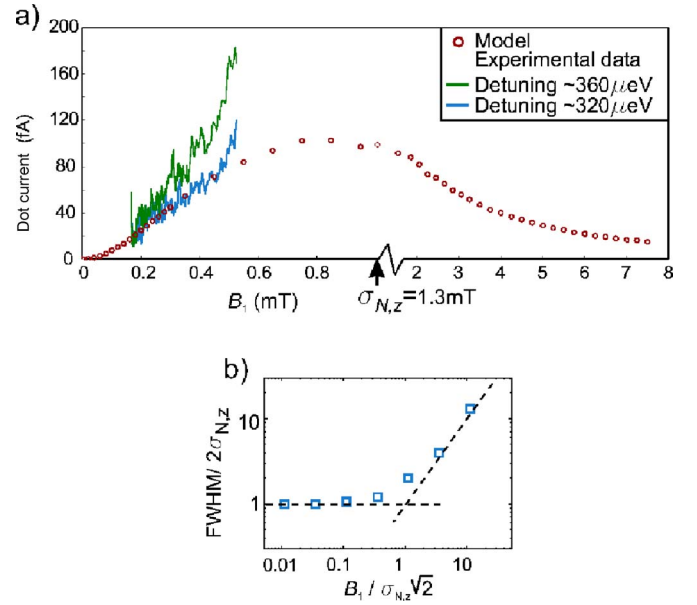
The ESR satellite peaks are visible for both resonant and

FIG. 5. Height and width of the ESR satellite peak. (a) Circles: calculated ESR peak height as a function of driving amplitude B_1. Parameters: $\hbar\omega = g\mu_B 100$ mT, $B_{ext}=100$ mT, $\sigma_N=2.2$ mT, $\Gamma_{L,R}=73$ MHz, $t=0.3$ μeV, $\hbar\Gamma_{in} = g\mu_B\sigma_N$, and $\Delta_{LR}=200$ μeV. Lines are the current measurements for two different values of Δ_{LR}. The measurements show time-dependent (telegraph-type) behavior. Therefore, the curves are obtained by repeating sweeps of B_1 and then selecting the largest current value for each value of B_1. (b) Calculated width of the ESR satellite peaks as a function of B_1. For small ESR power the peak is broadened by the random nuclear fluctuations; at high powers it is broadened by B_1.

inelastic transport regime [Figs. 4(a) and 4(b)]. For the resonant transport regime, we see that for $t/\sigma_N<5$ the satellite peaks increase in height when increasing t, simply because the coupling between the two singlet states increases. However, further increasing t reduces the signal, and this is because the exchange splitting then plays a more important role. Namely, increasing the exchange splitting reduces the mixing between the $|T_{11}^0\rangle$ state with the hybridized singlet state by the nuclear field gradient. This mixing is a crucial element for detecting the induced rotations of one of the two electron spins. In the inelastic transport regime, this exchange splitting is negligibly small and, therefore, the height of the satellite peak depends only on Γ_{in} and the driving field B_1.

A study of the height of the satellite peak as a function of B_1 reveals a nonmonotonous behavior, which can be seen in Fig. 5(a). The physical picture behind this behavior is most easily sketched by distinguishing three regimes:

(1) For $B_1 < \sigma_{N,z}$, for most of the nuclear configurations the spin in at most one of the two dots is on resonance, so spins are flipped in either the left or right dot. In that case, transitions are induced from, e.g., $|\uparrow\uparrow\rangle$ to $|\uparrow\downarrow\rangle = |S_{11}\rangle+|T_{11}^0\rangle$ or $|\downarrow\uparrow\rangle=|S_{11}\rangle-|T_{11}^0\rangle$. The resulting current flow initially increases quadratically with B_1, as one would normally expect [Fig. 5(a)].

(2) For $B_1 \gg \sigma_{N,z}$, for most of the nuclear configurations two spins are rotated simultaneously due to power broadening of the Rabi resonance. The stronger B_1, the more the transitions occur only in the triplet subspace (the driving field B_1 that rotates two spins dominates the $S-T_0$ mix-

ing by the nuclear spins). As a result, the current decreases for increasing B_1.

(3) If $B_1 \sim \sigma_{N,z}$ the situation is more complex because both processes (rotation of two spins simultaneously *and* transitions from $T_{11}^0\rangle$ to $S_{11}\rangle$) are effective. We find that if both processes occur with comparable rates, the overall transition rate to the singlet state is highest. This is the reason why the current has a maximum at $B_1 \approx \sigma_{N,z}$ [Fig. 5(a)].

The experimental data of the ESR satellite peak height (normalized by the zero-field current flow) for two different values of Δ_{LR} are shown in Fig. 5(a). In order to compare the experimental results with the model, we have estimated the rate Γ_{in} from the measured current flow at $B_{ext}=0$ (we found similar values for both curves). The agreement of the experimental data with the model is reasonable, as they show the expected quadratic increase with B_1, as well as a comparable peak height. However, we see that variations of the level detuning Δ_{LR} can result in considerable differences of the measured ESR peak height. We have two possible explanations for the deviations of the experimental data with the model. First, we have found experimental signatures of dynamic nuclear polarization when the ESR resonance condition was fulfilled. We expect that this is due to feedback of the electron transport on the nuclear spins (similar to that discussed in Refs. 11, 15, and 17), although the exact processes are not (yet) fully understood. Second, unwanted electric fields affect the electron tunneling processes, but are not taken into account in the model. We expect that these electric fields will not change the location and width of the ESR satellite peaks because this field does not couple the spin states. It is, however, possible that the height of the satellite peak is altered by the electric field because if can affect the coupling between $|S_{02}\rangle$ and $|S_{11}\rangle$.

Finally, we discuss the width of the ESR satellite peak [Fig. 5(b)]. If the inelastic tunneling process between the dots (with rate Γ_{in}) and B_1 are both smaller than $\sigma_{N,z}$, the ESR peak (obtained from simulations) is broadened by the statistical fluctuations of the effective nuclear field. For high B_1, the width approaches asymptotically the line with slope 1 [see Fig. 5(b)]. In this regime, the peak is broadened by the rf amplitude B_1. In the experiment,[1] the shape of the satellite peak was different (flat on top with sharp edges) than expected from the model. Furthermore, the FWHM was larger than expected from just $\sigma_{N,z}$. We attribute this to feedback of the ESR-induced current flow on the nuclear spin bath. As a result, a clear FWHM increase with B_1 could not be observed.

It should be noted that in the simulation the central peak is broader than the satellite peaks. From studying the influence of various parameters in the model, we conclude that the greater width of the central peak is caused by the transverse nuclear field fluctuations ($B_{N,x}$ and $B_{N,y}$), which broaden the central peak but not the ESR satellite peaks.

We conclude that the model discussed here qualitatively agrees with the main features that were observed in the double-dot transport measurements that aim at detecting (continuous wave) ESR of a single electron spin. The details of the ESR satellite peak height and width do not agree quantitatively with the model. We believe these deviations can be attributed to unwanted electric fields and feedback of the electron transport on the nuclear spin polarization. Improving the understanding of these feedback mechanisms remains interesting for future investigation, as it might point toward a direction to mitigate the decoherence of the electron spin.[12,18]

[1]F.H. L. Koppens, C. Buizert, K.-J. Tielrooij, I. T. Vink, K. C. Nowack, T. Meunier, L. P. Kouwenhoven, and L. M. K. Vandersypen, Nature **442**, 766 (2006).

[2]H. A. Engel and D. Loss, Phys. Rev. Lett. **86**, 4648 (2001).

[3]K. Ono, D. G. Austing, Y. Tokura, and S. Tarucha, Science **297**, 1313 (2002).

[4]A. C. Johnson, J. R. Petta, J. M. Taylor, A. Yacoby, M. D. Lukin, C. M. Marcus, M. P. Hanson, and A. C. Gossard, Nature **435**, 925 (2005).

[5]F. H. L. Koppens, J. A. Folk, J. M. Elzerman, R. Hanson, L. H. W. van Beveren, I. T. Vink, H. P. Tranitz, W. Wegscheider, L. P. Kouwenhoven, and L. M. K. Vandersypen, Science **309**, 1346 (2005).

[6]P.-F. Braun, X. Marie, L. Lombez, B. Urbaszek, T. Amand, P. Renucci, V. K. Kalevich, K. V. Kavokin, O. Krebs, P. Voisin, and Y. Masumoto, Phys. Rev. Lett. **94**, 116601 (2005).

[7]D. Gammon, A. L. Efros, T. A. Kennedy, M. Rosen, D. S. Katzer, D. Park, S.W. Brown, V. L. Korenev, and I. A. Merkulov, Phys. Rev. Lett. **86**, 5176 (2001).

[8]I. A. Merkulov, A. L. Efros, and J. Rosen, Phys. Rev. B **65**, 205309 (2002).

[9]A. V. Khaetskii, D. Loss, and L. Glazman, Phys. Rev. Lett. **88**, 186802 (2002).

[10]W. A. Coish and D. Loss, Phys. Rev. B **70**, 195340 (2004).

[11]K. Ono and S. Tarucha, Phys. Rev. Lett. **92**, 256803 (2004).

[12]O. N. Jouravlev and Y. V. Nazarov, Phys. Rev. Lett. **96**, 176804 (2006).

[13]R. de Sousa and S. Das Sarma, Phys. Rev. B **67**, 033301 (2003).

[14]D. Paget, G. Lampel, B. Sapoval, and V. I. Safarov, Phys. Rev. B **15**, 5780 (1977).

[15]J. Inarrea, G. Platero, and A. H. MacDonald (2006), e-print cond-mat/0609323.

[16]C. Poole, *Electron Spin Resonance*, 2nd ed. (Wiley, New York, 1983).

[17]M. S. Rudner and L. S. Levitov (2006), e-print cond-mat/0609409.

[18]D. Klauser, W. Coish, and D. Loss, Phys. Rev. B **73**, 205302 (2006).